Rendering Strategies for Underactuated Hand Exoskeletons

Mine Sarac, Massimiliano Solazzi, Miguel A. Otaduy, and Antonio Frisoli

***Abstract*—Underactuated exoskeletons offer improved simplicity, affordability, and movement adjustability based on interaction forces, but in turn they suffer from lack of controllability. In this letter, we propose different rendering strategies to improve the controllability of underactuated devices, with no prior knowledge about the task to be performed. Since underactuated devices cannot achieve all desired poses or render all desired forces, the proposed strategies replace these desired values with proxy values that the devices can satisfy. Strategies in the force and operational spaces aim to minimize the error between the desired and the actual output force or pose, respectively, during operation. We test these strategies first using an underactuated hand exoskeleton during a virtual grasping task. Then, we compare them to each other and to other existing methods by analyzing their control performance during a trajectory tracking task.**

***Index Terms*—Underactuation, hand exoskeleton, rendering rehabilitation robots, haptic systems.**

I. Introduction

HAND exoskeletons are widely used for rehabilitative, assistive and teleoperation applications [1]. Two important requirements in their design are ergonomics and safety, which are mapped to functional design specifications of reduced weight and bulk of the device. A common design approach is to align the mechanical centers of rotation with the finger joints, to prevent the generation of internal loads. However, this approach is challenging due to the high number of degrees of freedom (DoFs) of the hand. The alignment can be achieved by means of structures placed outside the phalanges, with remote centers of rotation or multi-loop mechanisms. However, these structures limit the wearability of the devices. Fully controlled exoskeletons control each finger joint independently, but suffer from high cost and mechanical complexity. Exoskeletons can be simplified by defining a relation between finger joints mechanically through additional mechanical adjustments or transmission units [2]–[5], or anatomically through fingertip connections [6]–[10].

An alternative solution for wearability is the concept of underactuation, i.e., to control multiple finger components using a single actuator based on interaction forces, instead of a strict joint ratio [11], [12]. Underactuated devices are highly favorable in terms of simplicity and affordability even if they cannot impose strict finger poses due to lack of controllability. Instead, they open/close fingers while the overall pose is determined based on the interaction forces. This behavior might be sufficient for rehabilitation tasks, but the lack of controllability complicates their use for haptic display.

Improving the controllability of underactuated devices for haptic display is currently an active research topic. Luecke [13] and Meli and Prattichizzo [14] developed different strategies for certain tasks using Cartesian devices, where all DoFs are independent. However, their strategies cannot be generalized to underactuated hand exoskeletons, where fewer actuators assist all DoFs in a coupled manner. Previously, Lobo *et al.* [15] developed a proxy-based rendering strategy for multi-dimensional haptic simulations, ensuring device passivity. Considering each interaction point between the virtual finger and virtual objects, their strategy can ensure inherent passivity. Even though this method is highly favorable for multi-dimensional environments, it is not efficient when the user's finger is modeled through rigid links and joints and the dimensionality of the system is reduced to $2-3\ DoFs$.

This letter defines two generic rendering strategies to minimize the error between the perceived and desired *(i)* force and *(ii)* pose. These strategies analyze the capabilities and the mechanical constraints of underactuated devices and adjust the output forces accordingly. We investigate their behavior in terms of finger pose and transmitted force using a hand exoskeleton during virtual grasping experiments. Finally, we compare the performance of these strategies and the previous proxy-based strategy [15] during a trajectory tracking task.

II. Underactuated Hand Exoskeletons

Underactuated hand exoskeletons are characterized by utilizing fewer actuators than the number of DoFs, by introducing extra mobility to the mechanism through passive joints and/or elastic elements [16]. Such extra mobility allows the mechanism to adjust its behavior automatically based on the interaction forces, while the user wearing the exoskeleton grasps objects with different shapes and sizes, as depicted in Fig. 1.

Manuscript received September 10, 2017; accepted February 8, 2018. Date of publication February 27, 2018; date of current version March 23, 2018. This letter was recommended for publication by Associate Editor K. Ogata and Editor K. Masamune upon evaluation of the reviewers' comments. This work was supported in part by the project "WEARHAP WEARable HAPtics for humans and robots" of the European Union Seventh Framework Programme FP7 under Grant 601165 and in part by the project "CENTAURO—Robust Mobility and Dexterous Manipulation in Disaster Response by Fullbody Telepresence in a Centaur-like Robot" of the European Union's Horizon 2020 Programme under Grant 644839. *(Corresponding author: Mine Sarac.)*

M. Sarac, M. Solazzi, and A. Frisoli are with the Perceptual Robotics, Scuola Superiore Sant'Anna, Pisa 56127, Italy (e-mail: mine.sarac@santannapisa.it; massimiliano.solazzi@santannapisa.it; antonio.frisoli@santannapisa.it).

M. A. Otaduy is with the Department of Computer Science Universidad Rey Juan Carlos, Madrid 28922, Spain (e-mail: miguel.otaduy@urjc.es).

Digital Object Identifier 10.1109/LRA.2018.2809916

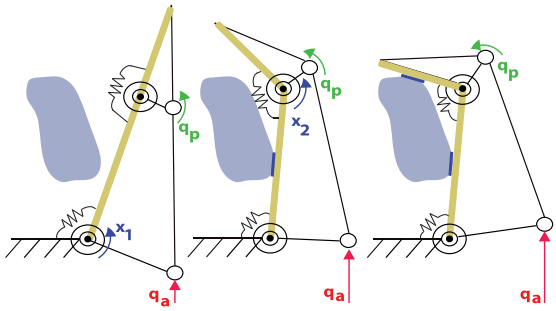

Fig. 1. Underactuated grasping concept using an underactuated system with 2 $DoFs$ and a single actuator: q_a, q_p and $\boldsymbol{x} = (x_1, x_2)^T$ represent the activities of actuated and non-actuated input joints and finger joints.

In particular, the exoskeleton is actuated to open/close the finger, while the finger joint rotations are modified by the physical contact between finger phalanges and objects. As a result, the user can perform complex grasping tasks using a single actuator.

A. Control Structure

The pose of a generic underactuated hand exoskeleton can be expressed using input joints as $\boldsymbol{q} = (\boldsymbol{q}_a, \boldsymbol{q}_p)^T$, where $\boldsymbol{q}_a$ and $\boldsymbol{q}_p$ represent the active (actuated) and passive (non-actuated) joints. The input forces that are supplied to the mechanism can be defined as $\boldsymbol{\tau} = (\boldsymbol{\tau}_a,\ \boldsymbol{\tau}_p)^T$ with active and passive components of input joints $\boldsymbol{q}$. Similarly, the finger joints $\boldsymbol{x}$ define the finger pose. The forces applied to the finger joints by the mechanism can be expressed as $\boldsymbol{\gamma}$, such that $dim(\boldsymbol{\tau}) = dim(\boldsymbol{\gamma}) > dim(\boldsymbol{\tau}_a)$ due to the underactuation. The Jacobian matrix $\boldsymbol{J} = (\boldsymbol{J}_a,\ \boldsymbol{J}_p)$ defines the kinematic mapping between exoskeleton and finger joints as

$$\dot{\boldsymbol{x}} = \boldsymbol{J}\ \dot{\boldsymbol{q}} = \begin{bmatrix} \boldsymbol{J}_a & \boldsymbol{J}_p \end{bmatrix} \begin{pmatrix} \dot{\boldsymbol{q}}_a \\ \dot{\boldsymbol{q}}_p \end{pmatrix}, \tag{1}$$

where $\boldsymbol{J}_a$ and $\boldsymbol{J}_p$ are the active and passive Jacobian components. The same Jacobian matrix can be used to map input and output forces as $\boldsymbol{\tau} = \boldsymbol{J}^T\ \boldsymbol{\gamma}$.

Underactuated hand exoskeletons can control neither the forces applied to finger joints, nor the finger pose. Alternatively, impedance control techniques might perform a force-based control using a reference for the finger pose. Impedance control is particularly useful because the underactuation concept also adjusts the output joint rotations based on contact forces. In particular, (2) computes the output force ($\boldsymbol{\gamma}_d$) that is necessary to reach a desired finger pose $\boldsymbol{x}_d$ from the actual pose $\boldsymbol{x}$, with a controllable stiffness matrix $\boldsymbol{K}_i = k\ \boldsymbol{I}_n$ to render the impedance control. Here, k is a scalar and I_n is the identity matrix.

$$\boldsymbol{\gamma}_d = \boldsymbol{K}_i\ (\boldsymbol{x}_d - \boldsymbol{x}). \tag{2}$$

The desired output forces $\boldsymbol{\gamma}_d$ are mapped into desired input forces $\boldsymbol{\tau}_d$ using the Jacobian $\boldsymbol{J}$ as

$$\begin{bmatrix} \boldsymbol{\tau}_{a\,d} \\ \boldsymbol{\tau}_{p\,d} \end{bmatrix} = \begin{bmatrix} \boldsymbol{J}_a^T \\ \boldsymbol{J}_p^T \end{bmatrix} \boldsymbol{\gamma}_d, \tag{3}$$

where $\boldsymbol{\tau}_{a\,d}$ and $\boldsymbol{\tau}_{p\,d}$ represent the desired force values that need to be applied by the active and passive input joints in order to achieve the desired forces $\boldsymbol{\gamma}_d$ along finger joints.

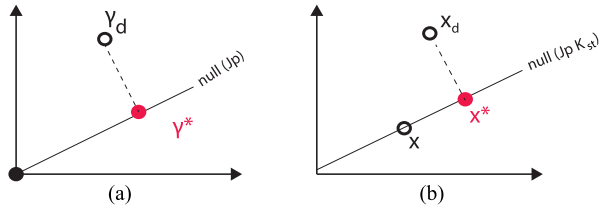

Fig. 2. Rendering algorithms for any instance of operation (a) in the force space, where proxy $\boldsymbol{\gamma}^*$ is the closest point to $\boldsymbol{\gamma}_d$ on $null(\boldsymbol{J}_p)$, which passes through the origin and (b) in the operational space, where $\boldsymbol{x}^*$ is the closest point to $\boldsymbol{x}_d$ on $null(\boldsymbol{J}_p\ \boldsymbol{K}_{st})$, which passes through an instant pose $\boldsymbol{x}$.

Using the desired values obtained through (3), the impedance controller can compute the PWM signals needed for the actuators using proportional (K_P) and integral (K_I) gains as $\boldsymbol{\tau}_{PWM} = K_P \boldsymbol{e}_\tau + K_I \int \boldsymbol{e}_\tau$, where $\boldsymbol{e}_\tau$ is the error between the actual and desired active forces ($\boldsymbol{e}_\tau = \boldsymbol{\tau}_{a\,d} - \boldsymbol{\tau}_a$). Meanwhile, the passivity of the non-actuated input joints defines their actual values as $\boldsymbol{\tau}_p = 0$ regardless their desired values $\boldsymbol{\tau}_{p\,d}$. In fact, the passivity of these non-actuated joints leads to a relation between applicable output joint torques as $0 = \boldsymbol{J}_p^T \boldsymbol{\gamma}$.

III. Rendering Strategies

Due to the passivity of non-actuated joints, nonzero values for $\boldsymbol{\tau}_{p\,d}$ cause the transmitted output forces $\boldsymbol{\gamma}$ to be different than the desired ones $\boldsymbol{\gamma}_d$. Even though this physical constraint cannot be overcome, rendering strategies can be developed to minimize the difference between the desired and exerted output forces by computing a proxy force ($\boldsymbol{\gamma}^*$) that satisfies the underactuation constraint $\boldsymbol{\tau}_p = 0$.

Fig. 2 represents two rendering strategies, one in force space and one in operational space. The strategy in force space computes a proxy force $\boldsymbol{\gamma}^*$ that satisfies the constraint with the closest distance to the desired force $\boldsymbol{\gamma}_d$. On the contrary, the underactuation constraint can be mapped to operational space by estimating the user's behavior based on his previous pose. The strategy in operational space computes a proxy pose $\boldsymbol{x}^*$ that can keep up this estimated behavior with the closest distance to the desired pose $\boldsymbol{x}_d$. The corresponding force $\boldsymbol{\gamma}^*$ is then computed using (2).

A. Rendering Strategy in Force Space

The minimization problem presented in Fig. 2(a) can be expressed mathematically as

$$\begin{aligned} &\boldsymbol{\tau}_a^* = \boldsymbol{J}_a^T\ \boldsymbol{\gamma}^*, \text{ with} \\ &\boldsymbol{\gamma}^* = \text{argmin}\ \frac{1}{2}\ \|\boldsymbol{\gamma}_d - \boldsymbol{\gamma}^*\|^2,\ \text{s.t. } \boldsymbol{J}_p^T\ \boldsymbol{\gamma}^* = \boldsymbol{0}, \end{aligned} \tag{4}$$

with closed-form expression

$$\boldsymbol{\gamma}^* = (\boldsymbol{I} - \boldsymbol{J}_p\ (\boldsymbol{J}_p^T\ \boldsymbol{J}_p)^{-1}\ \boldsymbol{J}_p^T)\ \boldsymbol{\gamma}_d. \tag{5}$$

The corresponding actuator forces ($\boldsymbol{\tau}_a^*$) can be calculated by merging (2), (4) and (5) as

$$\boldsymbol{\tau}_a^* = \boldsymbol{J}_a^T\ (\boldsymbol{I} - \boldsymbol{J}_p\ (\boldsymbol{J}_p^T\ \boldsymbol{J}_p)^{-1}\ \boldsymbol{J}_p^T)\ \boldsymbol{K}_i\ (\boldsymbol{x}_d - \boldsymbol{x}). \tag{6}$$

The virtual impedance displayed in the joint space with full DoFs under the control law in (6) can be expressed as

$$\frac{\partial \boldsymbol{\tau}}{\partial \mathbf{q}} = -\boldsymbol{J}^T \left(\boldsymbol{I} - \boldsymbol{J}_p \left(\boldsymbol{J}_p^T \boldsymbol{J}_p\right)^{-1} \boldsymbol{J}_p^T\right) \boldsymbol{K}_i \boldsymbol{J}. \tag{7}$$

If k is a scalar value, then the system has only negative or zero eigenvalues, hence it is intrinsically passive.

This rendering strategy in force space does not only calculate a proxy force $\boldsymbol{\gamma}^*$ that can be rendered by the underactuated device, but also ensures that the rendered force $\boldsymbol{\gamma}$ is closest to the desired one $\boldsymbol{\gamma}_d$. Doing so improves the perceived force around the finger joints, while the relationship between the reached and the desired finger pose is neglected. The force-space strategy should be highly favorable for haptic applications, where the main focus is the accuracy of the rendered forces.

B. Rendering Strategy in Operational Space

The extra mobility introduced by underactuation allows the finger to reach an infinite number of possible poses $\boldsymbol{x}$ for a given state of actuated joints $\boldsymbol{q}_a$, but prevents the finger joints to reach a strict pose. To improve the position performance of the system, we formulate a minimization problem similar to the strategy in force space, but expressed in terms of pose, as in Fig. 2(b). This problem requires the projection of the desired position onto the null-space of the matrix $\boldsymbol{J}_p \boldsymbol{K}_{st}$, where $\boldsymbol{K}_{st}$ is the stiffness matrix of the user's finger. This matrix can be estimated from previous finger activity as $\boldsymbol{K}_{st} = \frac{\partial \gamma}{\partial x}$. In practice, we use the difference between the current and the previous states of operation, i.e., $\frac{\Delta \gamma}{\Delta x}$. Assuming that the user does not change his behavior suddenly, the desired forces $\boldsymbol{\gamma}_{st}$ to cause the finger pose $\boldsymbol{x}$ to reach the desired pose $\boldsymbol{x}_d$ using the estimated joint stiffness $\boldsymbol{K}_{st}$ can be expressed as

$$\boldsymbol{\gamma}_{st} = \boldsymbol{K}_{st} \left(\boldsymbol{x}_d - \boldsymbol{x}\right). \tag{8}$$

The underactuated device cannot ensure that forces $\boldsymbol{\gamma}_{st}$ are transmitted to finger joints. Then, the minimization problem presented in Fig. 2(b) can be expressed using (2) as

$$\begin{aligned} &\boldsymbol{\tau}_a^* = \boldsymbol{J}_a^T \boldsymbol{K}_i \left(\boldsymbol{x}^* - \boldsymbol{x}\right), \text{ with} \\ &\boldsymbol{x}^* = \operatorname{argmin} \frac{1}{2} \left\|\boldsymbol{x}_d - \boldsymbol{x}^*\right\|^2, \text{ s.t. } \boldsymbol{J}_p^T \boldsymbol{K}_{st} \left(\boldsymbol{x}^* - \boldsymbol{x}\right) = \mathbf{0}. \end{aligned} \tag{9}$$

Simplifying the estimated stiffness as $\boldsymbol{K} = \boldsymbol{K}_{st}^T \boldsymbol{J}_p$, the closed-form expression is

$$\boldsymbol{x}^* = \boldsymbol{x}_d - \boldsymbol{K} \left(\boldsymbol{K}^T \boldsymbol{K}\right)^{-1} \boldsymbol{K}^T \left(\boldsymbol{x}_d - \boldsymbol{x}\right). \tag{10}$$

The corresponding actuator forces ($\boldsymbol{\tau}_a^*$) can be calculated by merging (8), (9) and (10) as

$$\boldsymbol{\tau}_a^* = \boldsymbol{J}_a^T \boldsymbol{K}_i \left(\boldsymbol{I} - \boldsymbol{K} \left(\boldsymbol{K}^T \boldsymbol{K}\right)^{-1} \boldsymbol{K}^T\right) \left(\boldsymbol{x}_d - \boldsymbol{x}\right). \tag{11}$$

It is important to note that the stiffness to be rendered can be defined for finger joints similar to the previous strategy. The virtual impedance displayed in the joint space with full DoFs under the control law in (6) can be expressed as

$$\frac{\partial \boldsymbol{\tau}}{\partial \mathbf{q}} = -\boldsymbol{J}^T \boldsymbol{K}_i \left(\boldsymbol{I} - \boldsymbol{K} \left(\boldsymbol{K}^T \boldsymbol{K}\right)^{-1} \boldsymbol{K}^T\right) \boldsymbol{J}. \tag{12}$$

Fig. 3. Multi-fingered underactuated hand exoskeleton.

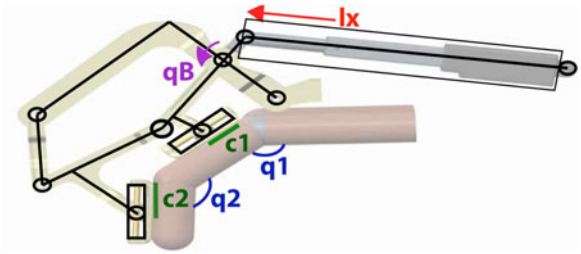

Fig. 4. Kinematic scheme of the underactuated finger exoskeleton.

Unlike the previous strategy, the estimated stiffness matrix K_{st} affects the eigenvalues of the virtual impedance directly, therefore stability cannot be ensured at all times. However, the estimated matrix could be adjusted such that the eigenvalues of the Jacobian matrix satisfy passivity.

The motivation behind the operational-space strategy is to minimize the distance between the reachable finger pose and the desired one. Doing so might improve the performance of position control algorithms, which can be highly favorable for rehabilitation applications, where the main focus is the accuracy of the pose.

IV. Experiments

The aforementioned control strategies have been tested experimentally using an underactuated hand exoskeleton, whose parameter values and kinematics analysis were detailed in previous work [12], shown in Fig. 3. Even though the hand exoskeleton was designed to support 5 fingers independently, this study is simplified for the index finger only.

The chosen hand exoskeleton can assist 2 $DoFs$ of the user's fingers through the displacement of a single linear actuator. Utilizing a linear actuator with mechanical gear box results in high output forces while sacrificing backdriveability. Not aligning the finger joints to the mechanical ones intentionally increases the adjustability of the device for various hand sizes. Compared to other underactuated devices, the novelty of the proposed device is to transmit only perpendicular forces to the phalanges, favoring the realism of interaction forces. In particular, the device utilizes passive linear sliders along finger phalanges with displacements c_1 and c_2 (see Fig. 4) so that tangential forces are not transmitted to the fingers. Suppressing tangential forces ensures that only perpendicular forces are applied to finger phalanges.

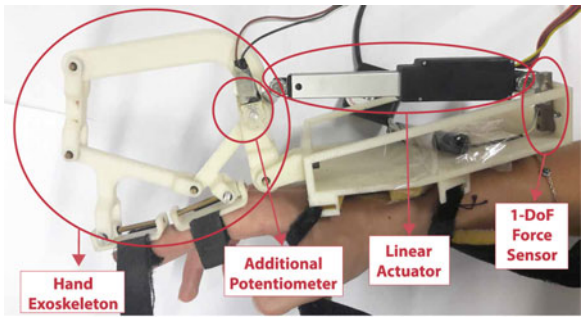

Fig. 5. Finger exoskeleton with additional potentiometer for pose estimation and force sensor for active backdriveability.

For the given exoskeleton system, the output joints can be defined as finger joint rotations $\boldsymbol{x} = (q_1, q_2)^T$, and the output forces can be expressed as joint torques $\boldsymbol{\gamma} = (\tau_1, \tau_2)^T$. The actuated and non-actuated joint displacement are defined as l_x and q_B. These definitions are depicted on the CAD model of a finger component as in Fig. 4.

The performance of the finger component is improved by implementing two additional sensors as shown in Fig. 5: *(i)* a potentiometer to measure the passive joint activity and estimate the finger pose through forward kinematics analysis [17], and *(ii)* a force sensor to measure the user's intention and open/close the finger accordingly through force control. Doing so, the device can achieve backdriveability to track the user's movements.

A. Experimental Scenarios

We have investigated experimentally the rendering strategies in force space and operational space during virtual grasping tasks. The virtual stiffness rendering task has been used to study: *(i)* the behavior of proxy and desired sets in force and operational spaces, *(ii)* the passivity of the overall system through sensed impedance, and *(iii)* the comparison between the proxy output forces $\boldsymbol{\gamma}_d$ and the actual interaction forces $\boldsymbol{\gamma}$. During the virtual interaction, the user is asked to lead the device with no real physical interaction, hence the trajectories of finger joints are expected to be different for each trial and user, and they cannot be compared to each other.

We have also compared the proposed strategies on a strict trajectory-tracking control experiment with healthy subjects, where the desired trajectory is ensured to be the same for all trials and users. In addition, we have added to the comparison the strategy in actuator space presented previously by Lobo *et al.* [15]. In this strategy, each interaction point between the virtual finger and the object is considered as a dimension, and these dimensions are mapped to proxy actuator forces using

$$\boldsymbol{\tau}_a^* = \boldsymbol{K}_q \, \boldsymbol{S} \, (\boldsymbol{J}^T \, \boldsymbol{J})^{-1} \, \boldsymbol{J}^T \, (\boldsymbol{x}_d - \boldsymbol{x}), \tag{13}$$

where $\boldsymbol{K}_q$ is the rendering impedance and $\boldsymbol{S}$ is the selection matrix to work only with the actuated components of the system. The rendering impedance in actuator space can be modeled as $\boldsymbol{K}_q = k \; avg(||\boldsymbol{J}_a||)^2$, where k is the same scalar as in (2). This strategy has the advantage of simplifying multi-dimensional systems to the actuator level, but it might not show great performance when dealing with rigid finger models.

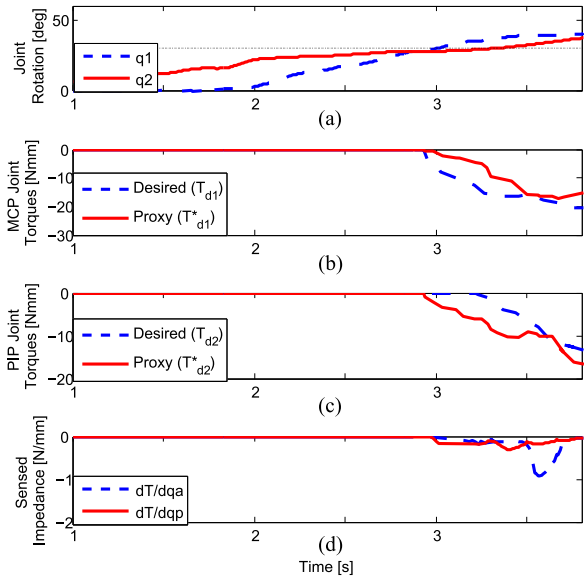

Fig. 6. Rendering strategy in force space.

Considering the objective of the optimization problem for the proposed strategies, the motivation for the trajectory-tracking experiment can be summarized by two aspects: *(i)* verify whether the force-space strategy is most favorable for minimizing the error between the desired and the actual forces $(\boldsymbol{\gamma}_d, \boldsymbol{\gamma})$ and *(ii)* verify whether the operational-space strategy is most favorable for minimizing the error between the desired and the actual pose $(\boldsymbol{x}_d, \boldsymbol{x})$.

B. Virtual Grasping Tests

In the virtual grasping test, a single user was asked to close his finger freely to reach a virtual object and squeeze it. The virtual grasping is defined by setting joint limits $\boldsymbol{x}_{lim}$, which were chosen as $(30°, 30°)^T$ for this experiment. The desired pose $\boldsymbol{x}_d$ is formed as (i) actual pose $\boldsymbol{x}$ before the virtual contact, and (ii) limit pose $\boldsymbol{x}_{lim}$ after the first contact. Doing so, the exoskeleton follows the user's intentions with high transparency before contact, and renders resistive forces representing the virtual interaction. Meanwhile, the controllable stiffness matrix K_i was intentionally kept low to allow the user to exceed the joint limits without applying excessively high forces.

1) Rendering in Force Space: Fig. 6(a) shows user's finger displacement $\boldsymbol{x}$ during virtual grasping with fixed joint limits $\boldsymbol{x}_{lim}$. The desired joint torques $\boldsymbol{\tau}_d$ and proxy torques $\boldsymbol{\tau}^*$ for MCP and PIP joints were calculated in real time using (2) and (5), based on desired and actual pose $\boldsymbol{x}_d$ and $\boldsymbol{x}$, and shown in Fig. 6(b) and (c) correspondingly. In particular, when the MCP joint reaches its limit, its desired torque starts to increase, while the desired torque for PIP is still 0. Meanwhile, the rendering strategy computes proxy torques, which are different from the desired ones. As the PIP joint reaches its limit too, the proxy and desired torque values are determined according to user's movements and the instant Jacobian. Fig. 6(d) shows that the device remains passive during the movement.

2) Rendering in Operational Space: Fig. 7(a) and (b) show the user's finger pose $\boldsymbol{x}$ and proxy pose $\boldsymbol{x}^*$ calculated using (10)

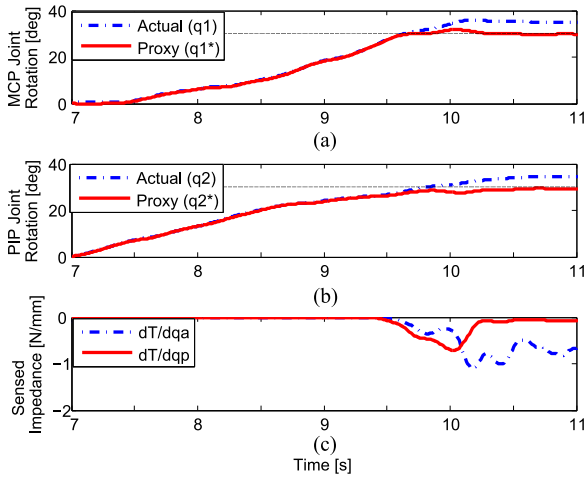

Fig. 7. Rendering strategy in operational space.

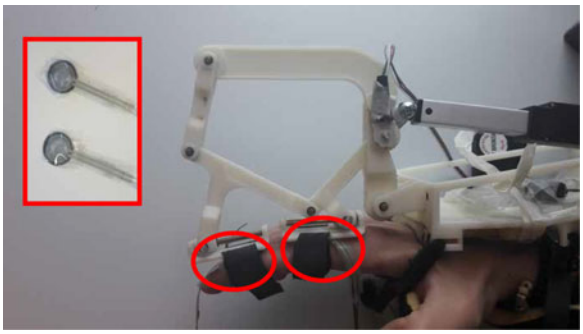

Fig. 8. FSR sensors between the device and the user's phalanges.

for the MCP (q_1) and PIP (q_2) joints respectively. In particular, when the MCP joint reaches its limit, the proxy pose for the joints is modulated differently to the desired pose. Fig. 7(c) shows that the device remains passive during the movement.

3) Discussion: These strategies aim to estimate the joint torques (γ^*) that can be rendered by the underactuated device. To verify whether the estimated forces could actually be perceived by the user, we inserted Force Sensing Resistor (FSR) sensors between the device and the user's finger phalanges (see Fig. 8) to measure the interaction forces. A silicon interface was attached between the FSR surface and the user's skin to improve the measurement quality.

FSRs measure the forces acting on the phalanges, and their readings (F_{FSR}) can be converted to joint torques as $\gamma_{FSR} = F_{FSR}./c$, where c represents the linear displacement of the corresponding phalange (see c_1, c_2 in Fig. 4). Fig. 9 shows the comparison between the actual and the proxy joint torques (a) in force space and (b) in operational space.

The average percentage of root mean square (RMS) error was found to be 1.9177% (0.962% and 1.659% for the MCP and the PIP joints) using the strategy in force space, and 1.7494% (1.357% and 1.104% for the MCP and the PIP joints) using the strategy in operational space. The RMS errors of the proposed strategies are found to be close to each other, so they cannot be claimed to be any better in terms of estimating the force transmission of the underactuated device.

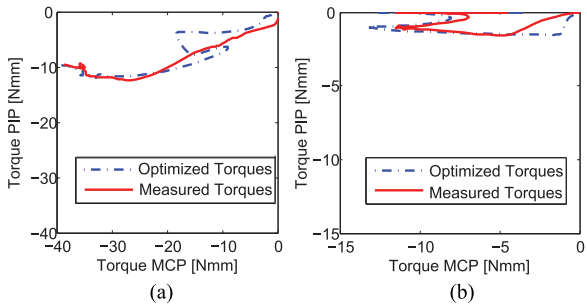

Fig. 9. Comparison between the calculated proxy and measured torques through FSR measurements.

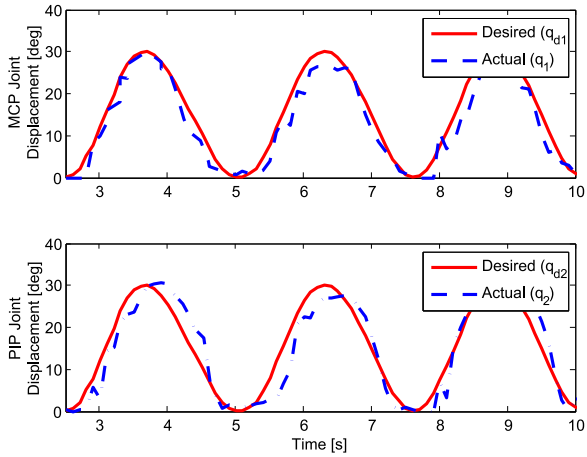

Fig. 10. Reference and actual joint displacement of one of the subjects.

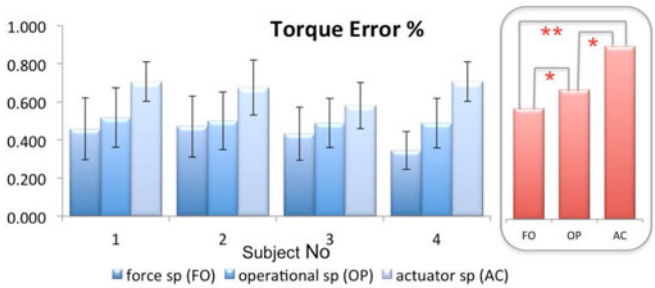

Fig. 11. Comparison of the error between desired and actual finger torques.

C. Trajectory Tracking Tests

In the trajectory-tracking feasibility test, 4 different subjects were asked to wear the device and test the strategies in force space, operational space, and actuator space for 3 cycles of a sinusoidal reference pose defined as the desired pose x_d. Fig. 10 shows this reference pose along with an actual pose recorded under the control strategy in the operational space. Since the finger exoskeleton opens/closes the finger according to the desired pose, the users were asked to stay relaxed.

The first motivation for this experiment was to compare the three rendering strategies based on the errors between the desired and the actual output forces. For each subject, the RMS values of torque errors ($\frac{\tau - \tau_d}{\tau_d}$) were calculated, as shown in Fig. 11 with their standard deviation depicted with arrows. A paired t-test was performed between these RMS values. The results were the following: between the strategies in force and

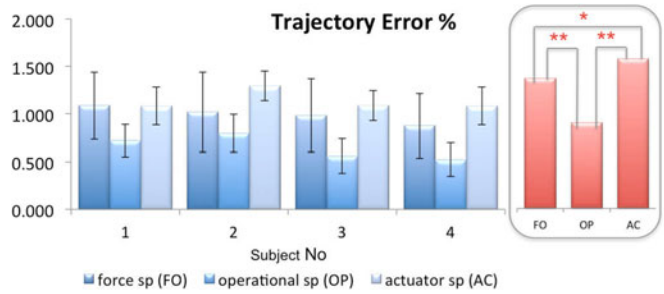

Fig. 12. Comparison of the error between desired and actual finger pose.

operational spaces, $p = 0.048$, in operational and actuator spaces, $p = 0.04$, and in force and actuator spaces, $p = 0.008$, which are depicted on the figure as (*) and (**). The strategy in force space seems to minimize the torque error significantly compared to the others.

The second motivation for this experiment was to compare the three rendering strategies based on the errors between the desired and the actual output pose. For each subject, the RMS values of trajectory errors ($\frac{\boldsymbol{q}-\boldsymbol{q}_d}{\boldsymbol{q}_d}$) were calculated, as shown in Fig. 12 with their standard deviation depicted with arrows. A paired t-test was performed between these RMS values. The results were the following: between the strategies in force and operational spaces, $p = 0.004$, in operational and actuator spaces, $p = 0.001$, and in force and actuator spaces, $p = 0.03$, which are depicted on the figure as (*) and (**). The strategy in operational space seems to minimize the trajectory error significantly compared to the others.

The rendering strategy in force space can render torques for finger joints similar to the desired values, while the strategy in operational space can control the finger joints to follow a reference finger pose better, despite the lack of controllability. Under these observations, the strategy in operational space might be useful for passive rehabilitation tasks where a strict trajectory can be given for finger rotations. Meanwhile, the strategy in force space might be effective for haptic applications or active rehabilitation tasks, where the user can move freely in the virtual environment and perceive the virtual interactions along finger joints in a realistic manner. Even though the strategy in actuator space [15] does not appear favorable for the given evaluation metrics, its advantages will increase as the dimensionality of the system grows.

V. Conclusion

This letter presents two alternative rendering strategies to improve the control performance of underactuated hand exoskeletons. Both strategies aim to calculate proxy values, which satisfy the underactuation constraints, and estimate the applicable transmitted forces. One strategy, derived in force space, improves the accuracy of perceived forces; while the other strategy, developed in operational space, improves the finger pose despite the lack of controllability. The feasibility of both strategies has been shown using an underactuated hand exoskeleton [12] during a virtual grasping task. They were compared to each other and to a strategy in actuator space [15], based on trajectory and torque errors during a trajectory-tracking control scenario. The statistical analysis between these three strategies showed that the strategy in force space renders forces closer to the desired ones, while the strategy in operational space moves finger joints closer to the desired trajectory.

Even though the rendering strategy in actuator space seems to have the worst performance compared to the strategies developed in this letter, it is important to note that the given evaluation metrics were chosen implicitly according to the objectives of the strategies developed in this letter. Therefore, a fair comparison between all three strategies in terms of perception needs to be conducted as future work.

References

[1] P. Heo, G. M. Gu, S.-j. Lee, K. Rhee, and J. Kim, "Current hand exoskeleton technologies for rehabilitation and assistive engineering," *Int. J. Precision Eng. Manuf.*, vol. 13, no. 5, pp. 807–824, 2012.

[2] M. Aiple and A. Schiele, "Pushing the limits of the cybergrasp for haptic rendering," in *Proc. 2013 IEEE Int. Conf. Robot. Autom.*, 2013, pp. 3541–3546.

[3] C. S. Tzafestas, "Whole-hand kinesthetic feedback and haptic perception in dextrous virtual manipulation," *IEEE Trans. Syst., Man, Cybern. A, Syst., Humans*, vol. 33, no. 1, pp. 100–113, Jan. 2003.

[4] M. Fontana, A. Dettori, F. Salsedo, and M. Bergamasco, "Mechanical design of a novel hand exoskeleton for accurate force displaying," in *Proc. IEEE Int. Conf. Robot. Autom.*, 2009, pp. 1704–1709.

[5] D. Ryu *et al.*, "Micro hydraulic system using slim artificial muscles for a wearable haptic glove," in *Proc. 2008 IEEE/RSJ Int. Conf. Intell. Robots Syst.*, 2008, pp. 3028–3033.

[6] P. Ben-Tzvi and Z. Ma, "Sensing and force-feedback exoskeleton (safe) robotic glove," *IEEE Trans. Neural Syst. Rehabil. Eng.*, vol. 23, no. 6, pp. 992–1002, Nov. 2015.

[7] M. Bergamasco, C. A. Avizzano, A. Frisoli, E. Ruffaldi, and S. Marcheschi, "Design and validation of a complete haptic system for manipulative tasks," *Adv. Robot.*, vol. 20, no. 3, pp. 367–389, 2006.

[8] F. Gosselin, T. Jouan, J. Brisset, and C. Andriot, "Design of a wearable haptic interface for precise finger interactions in large virtual environments," in *Proc. Joint Eurohaptics Conf. Symp. Haptic Interfaces Virtual Environ. Teleoperator Syst.*, 2005, pp. 202–207.

[9] O. Halabi and H. Kawasaki, "Five fingers haptic interface robot HIRO: Design, rendering, and applications," *Advances in Haptics*, M. H. Zadeh, Ed. InTech, 2010, doi: 10.5772/8691.

[10] P. Stergiopoulos, G. Moreau, M. Ammi, and P. Fuchs, "A framework for the haptic rendering of the human hand," in *Proc. 11th Symp. Haptic Interfaces Virtual Environ. Teleoperator Syst.*, 2003, pp. 340–347.

[11] I. H. Ertas, E. Hocaoglu, and V. Patoglu, "AssistOn-Finger: An underactuated finger exoskeleton for robot-assisted tendon therapy," *Robotica*, vol. 32, pp. 1363–1382, 2014.

[12] M. Sarac, M. Solazzi, E. Sotgiu, M. Bergamasco, and A. Frisoli, "Design and kinematic optimization of a novel underactuated robotic hand exoskeleton," *Meccanica*, vol. 52, pp. 749–761, 2016.

[13] G. R. Luecke, "Haptic interactions using virtual manipulator coupling with applications to underactuated systems," *IEEE Trans. Robot.*, vol. 27, no. 4, pp. 730–740, Aug. 2011.

[14] L. Meli and D. Prattichizzo, *Task-Oriented Approach to Simulate a Grasping Action Through Underactuated Haptic Devices*. Berlin, Germany: Springer, 2014, pp. 249–257.

[15] D. Lobo, M. Sarac, M. Verschoor, M. Solazzi, A. Frisoli, and M. A. Otaduy, "Proxy-based haptic rendering for underactuated haptic devices," in *Proc. IEEE World Haptics Conf.*, 2017, pp. 1–6.

[16] T. Laliberte, L. Birglen, and C. Gosselin, "Underactuation in robotic grasping hands," *Mach. Intell. Robot. Control*, vol. 4, no. 3, pp. 1–11, 2002.

[17] M. Sarac, M. Solazzi, D. Leonardis, E. Sotgiu, M. Bergamasco, and A. Frisoli, *Design of an Underactuated Hand Exoskeleton With Joint Estimation*. New York, NY, USA: Springer, 2017, pp. 97–105.